Article

Not peer-reviewed version

Role of Phase Information Propagation in the Realisation of Super-resolution Based on Speckle Interferometry

Yasuhiko Arai *

Posted Date: 27 October 2023

doi: 10.20944/preprints202310.1775.v1

Keywords: Super-resolution; Speckle interferometry; Zero-order diffracted light: Phase information.

Article

Role of Phase Information Propagation in the Realisation of Super-Resolution Based on Speckle Interferometry

Yasuhiko Arai

Kansai University; arai-kansai-u.ac.jp

Abstract: Super-resolution technology is important not only in bio-related fields but also in nanotechnology, particularly in the semiconductor industry, where fine patterning is required and super-resolution is essential. However, observing microstructures beyond the diffraction limit proposed by Abbe and Rayleigh is considered impossible because of diffraction in traditional optical microscopy observation techniques. However, in recent years, it has been possible to observe microstructures beyond the Rayleigh criterion by analysing the phase distribution of light. This study investigated the physical reasons why phase analysis makes this new analysis technique possible using simulations. The results confirmed that the phase component of the zero-order diffracted light reflected from the microstructure and able to pass through the lens system contained the phase information related to the shape of the measured object. Analysis of this information demonstrates the possibility of realising super-resolution based on speckle interferometry.

Keywords: super-resolution; speckle interferometry; zero-order diffracted light; phase information

1. Introduction

Since the 2014 Nobel Prize in Chemistry was awarded to PALM [1] and STED [2,3] using fluorescent proteins by E. Betzig, W. E. Moerner, and S. W. Hell, super-resolution technology in biotechnology has become an important technology to support further human development [4–11]. It is also an important technology in the semiconductor industry, where much finer patterning is required in the field of nanotechnology [12,13].

However, as shown by Abbe [14] and Rayleigh [15,16], it has been proposed that image acquisition by TV cameras, which can capture 2D information instantaneously, is limited in the observation of microstructures due to the diffraction limit as a lens property. According to the Rayleigh criterion based on this idea, structures finer than approximately half the wavelength of the light source used for observation cannot be observed using a lens system.

However, a new super-resolution technique based on speckle interferometry that analyses the phase distribution of light was recently proposed by Arai [17]. The new analysis process in this technique is fundamentally different from the traditional technique proposed by Abbe and Rayleigh for analysing the intensity distribution of light.

It is now known that phase analysis techniques using a laser beam can easily detect the phase distribution of light with high resolution, including fringe scanning techniques using light interferometry [18,19]. It is also well known that speckle interferometry is an excellent measurement technique, especially when the measurement object is a structure with a rough surface, where high measurement resolution can be expected [20].

In this study, the distribution of the phase of light in an optical system and the physical properties of the phase distribution used to achieve super-resolution in the Arai method were investigated using electromagnetic field simulation [21]. Consequently, the mechanism for achieving super-resolution was physically clarified.

Preprints (www.preprints.org) | NOT PEER-REVIEWED | Posted: 27 October 2023 doi:10.20944/preprints202310.1775.v1

2. Materials and Methods

2.1. Principle of measuring microstructures beyond the diffraction limit based on speckle interferometry technology

Assuming, for example, that the measurement cross-section of the measurement object shown in Figure 1(a) can be expressed as f(x) and that a lateral shift δx is assigned to the measurement object, as shown in Figure 1(b), the shape displacement occurring at each measurement point can be expressed as f(x+δx) - f(x). The displacement of the shape at each of these points is then accurately measured using the speckle interferometry [20,22,23], and the pseudo-differential value {f(x)-f(x+δx)}/δx in the shift direction with respect to the shape is obtained by dividing the detected displacement with the transverse shift amount. Furthermore, the shape of the measurement object can be reconstructed by integrating the pseudo-differential value [17,21].

Through this computational process, structures beyond the diffraction limit were observed. Speckle interferometry is a method for detecting the amount of deformation with high resolution by capturing image information before and after the deformation of the measurement object [18,20]. Therefore, speckle interferometry is a suitable analysis method for detecting the shape displacement f(x+δx)-f(x) at each measurement point on the measuring object because of the lateral shift of the measuring object at a high resolution in this study. This property was applied to the super-resolution technique in this study [17].

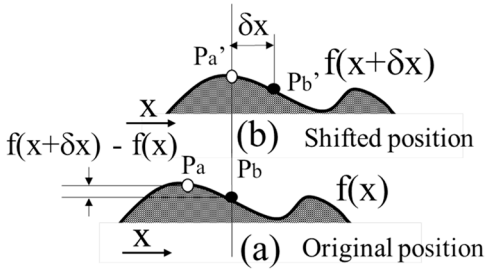

Figure 1. Principle of analysing method. (a) Section of measured object at original position; (b) Section of measured object at shifted position.

2.2. Observation optics

The basic optical system used in this experiment, which is based on speckle interferometry, is shown in Figure 2. This optical system uses a laser with a wavelength of 532 nm and an output of 100 mW as the light source and a Mitsutoyo (M Plan Apo 200x manufactured) objective lens.

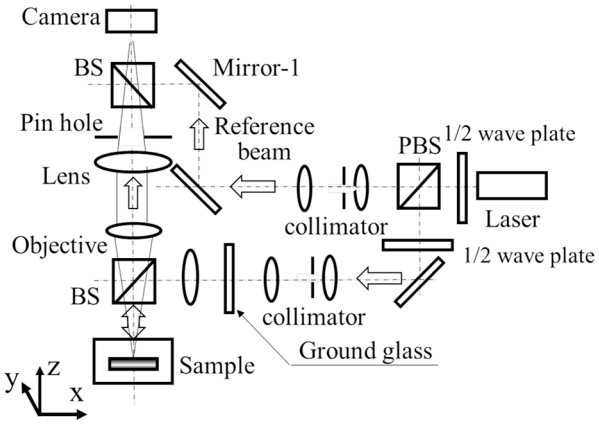

Figure 2. Experimental optical system.

This lens had a magnification of 200x and a numerical aperture of 0.62, which provided a diffraction limit of 660 nm. The camera has an image element spacing of 1.6 μm and a pixel size of 1024 x 1024. and 4096 grey levels [17]. Furthermore, the use of plane waves as the reference light of

Preprints (www.preprints.org) | NOT PEER-REVIEWED | Posted: 27 October 2023 doi:10.20944/preprints202310.1775.v1

the speckle interferometer enables deformation measurements to be performed using only two speckle patterns before and after deformation. This has been demonstrated in previous reports [17,22–24].

2.3. Simulation of the analysis in the observation of microstructures based on phase analysis

2.3.1. Simulation model

In general, it is extremely difficult to eliminate disturbances such as stray light in an optical system completely when using an actual optical system to verify and confirm the principle, as attempted in this study. In addition, it is difficult to discuss the physical phenomena in detail because of limitations such as measurement accuracy and the experimental environment.

To avoid these problems, the current study uses an electromagnetic field simulation software (COMSOL Multiphysics) to investigate the physical phenomena in which the observation of microstructures beyond the diffraction limit is achieved using a new super-resolution technology based on speckle interferometry techniques [21,25]. The computer simulation model used in a previous report [25], shown in Figure 3(a), was used as the optical system model in this study.

In the optical system used for the experiment shown in Figure 2, an experiment was performed by analysing the light reflected from a glass reflective diffraction grating as a measurement sample [17]. Because this study investigates the physical interpretation of the properties of the phase distribution of light from microstructures beyond the diffraction limit in super-resolution speckle interferometry techniques, the measurement object was used as a simplified model compared with the treatment in previous reports [21,25].

Specifically, the shape was set as a simple sample modelled by supplying a group of spherical wave point sources with a phase distribution depending on the shape given to the reflected light from each point on the measurement object. In other words, when the measurement object is a flat plane, as shown in Figure 3(b), it is modelled by assuming that spherical wave light sources with the same phase are aligned on the same plane. When a surface with protrusions/steps is to be measured, a spherical wave light source with the wavelength of the light source as 2π rad to correspond to the height of the protrusions and with the phase given according to the shape is placed as the protrusions, thus expressing the shape of the protrusions as a phase distribution.

In the simulation model shown in Figure 3(a), the mesh size was set by considering the load on the computer memory, as in a previous report [25]. In other words, 1/12 of the wavelength was set as the mesh size as a condition under which the influence of the mesh size did not extend to the calculation results as far as possible. Under these conditions, it was confirmed that the calculation results did not change even if the mesh was not engraved any finer. The arrangement of the light sources as measurement objects is also set with a minimum unit spacing of 0.1 nm, considering the load on the computer's memory. To make effective use of the limited memory, the parallel side walls and the right-side wall of the computational domain were defined as perfectly matched layers (PML). In creating the simulation model, as in a previous report [25], the computational domain was defined with the minimum possible memory (memory capacity of 2 TB) to minimise the load on memory capacity.

The light source used in the simulation is a spherical wave source derived from Maxwell equations defined by Eq. (1) [25]. In the light source model shown in Eq. (1), Va is the electromagnetic field intensity, λ is the wavelength, and ϕ is the initial phase of the light from the source. The distribution based on this phase ϕ is used to set the shape of the measurement object as described above.

$$E = V_a \times \frac{\exp\{i(2\pi/\lambda \sqrt{x^2 + y^2} + \phi)\}}{\sqrt{x^2 + y^2}} \quad (1)$$

Preprints (www.preprints.org) | NOT PEER-REVIEWED | Posted: 27 October 2023 doi:10.20944/preprints202310.1775.v1

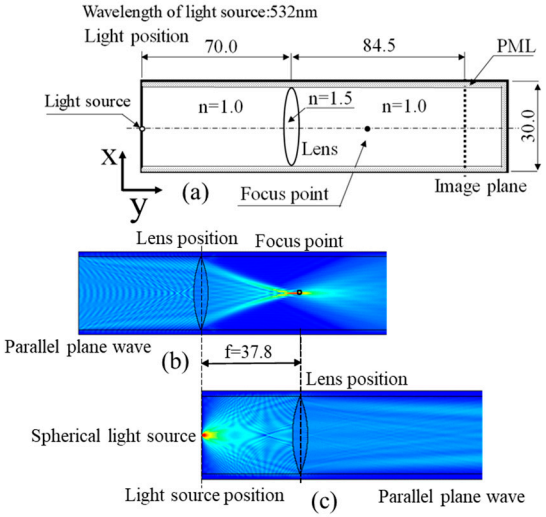

Figure 3. Simulation model. (a) Optical system in simulation approach; (b) Relation between parallel plane wave and focus distance; (c) Relation between light source and lens.

The specific optical elements used in the simulation model were modelled by assuming the objective lens to be a thin biconvex lens and defining the refractive indices of air and the lens to be 1.0 and 1.5, respectively. First, the focal lengths and diffraction limits of the lenses of the optical system were identified.

The focal length (f = 37.8 μm) was determined by setting the lens focal point as the point where the highest intensity of the electromagnetic field is focused by the lens when the plane wave as a collimated light is irradiated by the lens from the left wall surface, as shown in Figure 3(b). Furthermore, the focal length f was confirmed as 37.8 μm by setting the spherical wave source on the optical axis of the left wall surface, as shown in Figure 3(c), and confirming that the electromagnetic field intensity after passing through the lens is parallel light when the lens is set at a distance from the left wall surface by the lens focal length determined using Figure 3(a).

In general, the lens used here is designed by a glass with a refractive index of 1.5 by a circular arc of radius 40 μm. As both convex surfaces of the lens are formed by arcs of radius 40 μm, the focal length can be obtained as 40 μm if the thickness of the lens is sufficiently thin [21,25].

However, in this study, the focal length is determined by a procedure using the relationship between the actual collimated light and the lens, as shown in Figure 3, because the thickness of the lens is not necessarily sufficiently thin (5.83 μm relative to the lens diameter). Consequently, the NA of the objective lens can be estimated as 0.37 [= 1 x sin ($\tan^{-1}$ (15/37.8))]. The diffraction limit as a Rayleigh criterion can then be obtained as 877 nm (=0.61×λ/NA=0.61×532/0.37). The characteristics of this optical system were based on the results discussed in a previous report [25] and were also used in this study.

2.3.2. Verification of the Rayleigh criterion in the diffraction limit

In the optical system shown in Figure 3, when the spherical-wave light sources shown in Eq. (1) are placed at symmetrical positions across the optical axis on a plane 70 μm away from the lens, 2 μm separated from each other and the phase ϕ of the two light sources are both 0 rad, the light from the two light sources shown in Figure 4(a) interferes and forms Young fringes because it does not exceed the diffraction limit.

Preprints (www.preprints.org) | NOT PEER-REVIEWED | Posted: 27 October 2023 doi:10.20944/preprints202310.1775.v1

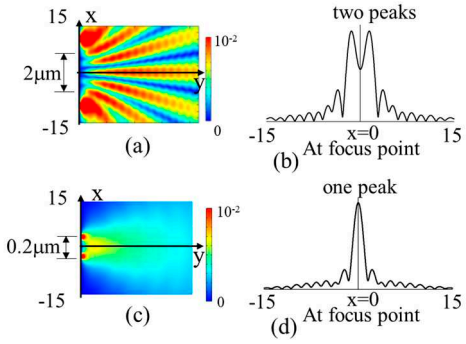

Figure 4. Relation between distance of two light sources and diffraction. (a) The distance between the two light sources is greater than the diffraction limit. (b) Two peaks in the case of non-diffraction. (c) The distance between the two light sources is shorter than the diffraction limit. (d) One peak in the case with diffraction.

A part of Young's fringes passes through the lens, as shown in Figure 5(a), which shows the two-dimensional distribution of the electromagnetic field intensity, and the bright spots can be observed as two points with two intensity peaks on the imaging plane, as shown in Figure 4(b).

Conversely, if the phase is 0 rad when the distance between the two light sources shown in Figure 4(c) is 0.2 μm, the light from the two light sources does not reach the lens except for the zeroth-order diffracted light along the optical axis, as shown in Figure 6(a), which shows the two-dimensional distribution of the electromagnetic field intensity.

In this case, only the zeroth-order diffracted light along the optical axis reaches the lens because the two light sources are beyond the diffraction limit.

Consequently, as shown in Figure 4(d), the intensity distribution on the image plane becomes a single point, which means that, in this case, it cannot be observed as two bright points.

Thus, it can be confirmed that the diffraction-limited phenomenon, in which the observation as two points becomes impossible depending on the wavelength and distance of the light source, can also be realised in the simulation, as shown in Figure 4.

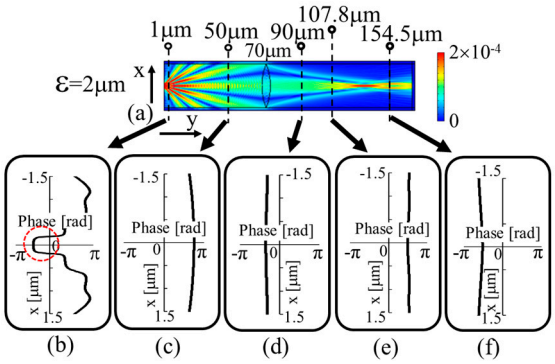

Figure 5. Phase distribution at each measurement point (ε=2μm). (a) Distribution of electromagnetic field strength. (b) Phase distribution at 1 μm. (c) Phase distribution at 50 μm. (d) Phase distribution at 90 μm. (e) Phase distribution at 107.8 μm (focal point of this lens). (f) Phase distribution at 154.5 μm (image plane of this lens).

Preprints (www.preprints.org) | NOT PEER-REVIEWED | Posted: 27 October 2023 doi:10.20944/preprints202310.1775.v1

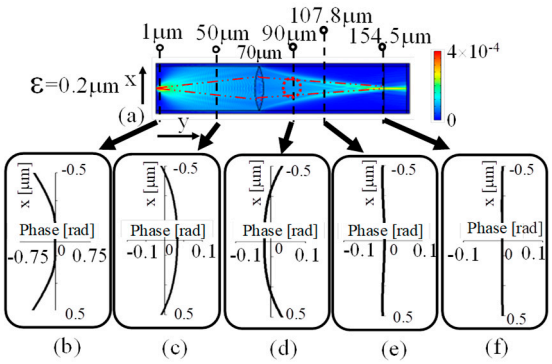

Figure 6. Phase distribution at each measurement point (ε=0.2μm). (a) Distribution of electromagnetic field strength. (b) Phase distribution at 1 μm. (c) Phase distribution at 50 μm. (d) Phase distribution at 90 μm. (e) Phase distribution at 107.8 μm (focal point of this lens). (f) Phase distribution at 154.5 μm (image plane of this lens).

In this case, as shown in a previous report [25], even if the distance between the two light sources is close beyond the diffraction limit, if the phases of the two light sources are shifted by π rad, they can be observed as two bright points instead of as a single point as the Rayleigh criterion suggests. Furthermore, this phenomenon has been confirmed by other institutes [26–28].

3. Results and Discusion

3.1. Observation results of diffraction gratings beyond the diffraction limit

The results of the observation of a reflective diffraction grating with a periodic structure of 278 nm, in which the period observed by SEM exceeded the diffraction limit, are shown in Figure 7(a). Furthermore, this method can not only observe the microstructure of the repeating structure shown in Figure 7 but can also capture shaped structures as three-dimensional, such as microspheres [23] and microcharacters [20], as reported previously.

In contrast, the results shown in Figure 7(b) indicate a slightly magnified period compared to the SEM observation results. Because this study was not based on traditional observation techniques and the object was not observed by focusing the object on the imaging plane, the phenomenon of this magnification change could not initially be interpreted clearly with regard to the observation magnification of the lens. However, the current simulation also examined the phenomenon of changing the magnification.

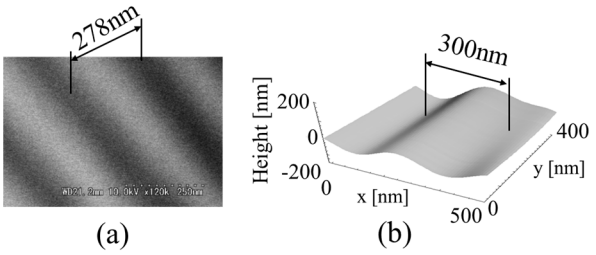

Figure 7. Measured object and measured result. (a) SEM image of diffraction grating (period: 278nm). (b) Measured result.

3.2. Phase distribution at each point on the optical axis in the case of exceeding the diffraction limit by simulation

The state of the phase distribution of the light from the microstructure beyond the diffraction limit at each point on the optical axis in relation to the two light sources and their distances was then verified by simulation.

 doi:10.20944/preprints202310.1775.v1

Figure 5(a) illustrates the two-dimensional distribution of the electromagnetic field intensity near the optical axis for two light sources with a distance of 2 μm between two points that do not exceed the diffraction limit when the phase is both 0 rad. At 1 μm, immediately after emitted from the light source, the lights interfere as shown by the red dashed line in Figure 5(b), which generates the phase distribution in the x-direction. It can be noted that the light is a plane wave with a flat phase depending on the beam width as a beam along the optical axis.

As shown in Figure 5(a), this interfered zero-order diffracted light travels towards the lens with a slight spread along the optical axis. Consequently, as shown in Figure 5(c), at 50 μm from the measurement object, the phase distribution of the zero-order diffracted light grows into a spherical wave whose phase is slightly delayed as it travels away from the optical axis because the light source itself is set as a spherical wave.

After passing through the lens at 90 μm, as shown in Figure 5(d), the direction of convexity of the phase distribution changes so that the phase distribution at 50 μm is reversed by the lens. The phase advances at the periphery, away from the optical axis. It is shown that the light itself becomes a wavefront focused towards the focal point.

Then, at 107.8 nm in the back focus of the lens, the phase was almost flat near the optical axis, as shown in Figure 5(e). Furthermore, on the image plane in Figure 5(f), the phase distribution is found to be slightly spherical and convex in the direction of travel.

However, when the phases of the two sources shown in Figure 6(a) are both 0 rad and their distance is 0.2 μm, the phase distribution does not become like the zero-order diffracted light of the Young fringe as it does when the diffraction limit of Figure 5(a) is not exceeded. In that case, the phase is delayed in the periphery with a symmetrical phase distribution across the optical axis in Figure 6(b), which shows the state at 1 μm immediately after the light source. It can be observed that the light wave is largely spread out.

However, in Figure 6, Young's fringe interference fringes cannot be observed, as shown in Figure 5. Therefore, light from the two light sources diffuses immediately in the transverse and travelling direction near the light source. As a result, the change in the phase distribution of light in the direction of travel was small, and the phase distribution was averaged.

For this reason, the maximum and minimum values of the phase distribution in the direction of travelling y are ±0.1 rad as much smaller values in Figure 6, compared to the values of π rad and -π rad in the case of Figure 5. These indicate that the state of the spread of the phase distribution is clearly different when the distance between the light sources exceeds the diffraction limit and when it does not.

At the 50 μm position shown in Figure 6(c), where the light has progressed further from Figure 6(b), the phase is delayed at the position away from the optical axis and the range of the peripheral phase delay is expanded as a spherical wave with a broad spread. At the 90 μm position shown in Figure 6(d) after the lens has passed through, contrary to Figure 6(c), the phase at the periphery away from the optical axis increases and the phase distribution becomes a wavefront (phase distribution) that focuses towards the rear focal point. At the back focus of the lens, as shown in Figure 6(e), the phase is a flat plane wave on the optical axis. At the imaging plane, Figure 6(f), it can be noted that the phase is again a plane wave with a flatter phase. This state indicates that when lights from two light sources exceeding the diffraction limit are captured on the image plane, as shown in a previous study [25], a phenomenon occurs that is in agreement with the results obtained when the phase is spatially flattened on the image plane, even if the phases of the two light sources are different.

Thus, if the phase is spatially flattened on the image plane, it can naturally be understood that the phase difference between the two points to be measured cannot be detected by observing the phase distribution on the image plane. However, it has been confirmed that in actual optical systems, as shown in Figure 2, when a three-dimensional shape exists on the measurement object, the phase distribution can be detected, and the shape of the object can be reconstructed as a phase distribution, as shown in Figure 7.

It should be noted that the experiments did not use spherical waves with phase-aligned wavefronts, as in the simulations. In other words, scattered light with wavefronts of random phase

 doi:10.20944/preprints202310.1775.v1

is used in the experiment. In addition, it should be noted that the phase distribution is not detected at the image formation position of Figure 6 (a) in the simulation.

However, in the current experiment, the phase information was detected at a position that was not too close to the objective lens. Based on the experimental situation, it was also decided to detect the phase in the simulation at a position not too close to the objective lens and at a position where the phase changed significantly in the x-axis direction with respect to the direction of light travel. As a position suitable for this condition, the phase was detected at 90 μm shown in Figure 6(d), which is considered to be able to detect the phase information on the measured object as unaffected by the surroundings as possible.

3.3. Phase analysis in the area between the lens position and the posterior focal point

The distribution of the electromagnetic intensity in Figure 6(a) shows that when the distance between the two light sources is 0.2 μm, which is beyond the diffraction limit, the light from the light source passes through the lens while only the zeroth-order diffracted light spreads slightly radially from the light source. In other words, light from the light source spreads radially as a spherical wave immediately after it is emitted, as shown in Figure 6(b) and (c). To obtain information on a spread of light using its intensity distribution, the light is focused again using a lens to form an image of the object, which is then observed as an image. However, in the analysis using the phase distribution, when the spreading light is refocused, the phase changes according to the length of the optical path through which the light has passed are superimposed on the phase distribution containing information concerning the shape of the original measurement object in the vicinity of the optical axis. Consequently, it may be difficult to detect the phase accurately based on the original shape of the measurement object.

It is thought that the effect of the optical path length of the spreading light may cause the original information to be hidden in the phase distribution owing to this problem in a new optical path length.

Therefore, it is essential to capture only the light near the optical axis of the zeroth-order diffracted light, which has as little spread as possible and is not focused by the lens in cases such as those shown in Figure 6(a). In actual optical systems, the principle of measurement is based on speckle interferometry. Therefore, it is believed that the light incident on the lens is only detected near the optical axis passing through the pinhole. In other words, if only light on an optical axis parallel to the optical axis is detected as far as possible in Figure 6(a), such that no additional phase element owing to differences in the optical path is added to the phase distribution of the measurement object, the observation of the phase distribution may be close to the experimental results using actual optical systems. However, it was assumed that the COMSOL used in this simulation would facilitate a pinhole setting by placing a wall with a PML setting just in front of the lens. However, the light reflected from the pinhole wall caused complex multiple reflections in the optical system because the PML settings cannot be sufficiently set up. In other words, the problem is that the pinhole setting cannot be always perfect. Therefore, it was decided here to perform a simpler process, instead of a pinhole-based simulation, by capturing only the light on the optical axis as far as the area indicated by the red dashed circle in Figure 6(a) at 90 μm shown in Figure 6(d), as the pinhole-based simulation is currently difficult to perform.

Under the conditions of this information collection, as shown in Figure 8, two light sources (Figure 8(a)) and three light sources (Figure 8(b)) are assumed in this study. In this case, the distance between the light sources is set to ε μm, and the phase of each light source is set to α, β. Furthermore, using the knowledge that 2π rad corresponds to the light source wavelength of 532 nm, the position of the light sources is set approximately by changing the value of the phase. Specifically, it was decided to treat the light as approximated as coming from a source one-half of a wavelength in front (266 nm) when the phase advances by π rad. The spherical wave from the light source set up in this way passed through the lens, and the phase at a position at 90 μm (furthermore, the phase difference was converted into a length using the wavelength-phase relationship) was observed. In the optical system used in the experiments, the phase distribution of the object light was detected with high resolution based on the spatial fringe analysis method by interfering with the object light from the

Preprints (www.preprints.org) | NOT PEER-REVIEWED | Posted: 27 October 2023 doi:10.20944/preprints202310.1775.v1

object and a plane wave as the reference light [17]. Based on this processing approach, in the simulation, the wavefront corresponding to the reference light is calculated in advance as the phase distribution when both phases α and β of each light source in Figure 8 are set to zero. By subtracting such a reference phase distribution from the phase distribution obtained by setting α and β, only the phase distribution originally intended to be obtained is calculated.

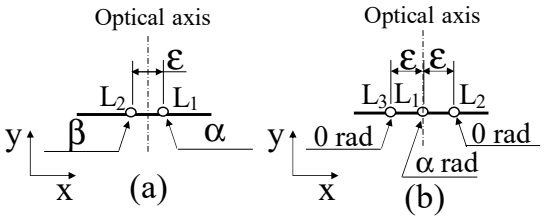

Figure 8. Position of light sources in simulation. (a) In the case of two light sources. (b) In the case of three light sources.

3.4. Simulation of two light sources with different phases

One of the phases α and β of the two light sources separated by $\varepsilon = 0.2$ μm shown in Figure 8(a) was set to 0 rad, while the other was set to phase in the range of angles $\pi/4$, $\pi/2$, and $3\pi/4$ in the first and second quadrants, where the phase change in the phase plane is relatively small.

As a result of using this condition, information on the simpler nature of the state, which is close to linearity, eliminating the complex nature, it is considered that the nature of the phase distribution beyond the diffraction limit, which is the purpose of this study, can be successfully verified by observing it without complicating it. As a concrete matter of consideration, it was examined whether the phase distribution of the wavefront detected at 90 μm when one of the values of α and β is set to 0 rad and the other changes to $\pi/4$, $\pi/2$, and $3\pi/4$ rad.

Figure 9(a) shows the phase distribution when both α and β are set to 0 rad. This condition is used as the standard phase distribution for the reference beam. In the experiments, speckle interferometry was used to determine the displacement $f(x+\delta x) - f(x)$ at each measurement point when the object was laterally shifted by performing a calculation between the two measurement points of the object. Based on the above concept, to determine the amount of change $\varphi\alpha\beta$ when one of α and β was changed by 0 and the other by $\pi/4$, $\pi/2$, and $3\pi/4$ rad, respectively, the phase distribution $\varphi 00$ when both α and β are set to 0 rad was obtained in advance. The value of $\varphi 00$ was then subtracted from the value when one of them is changed by $\pi/4$, $\pi/2$, and $3\pi/4$ rad, respectively. This processing accurately detects the phase change $\varphi\alpha\beta$ associated with a change in α and β.

Furthermore, the phase distribution in Figure 9(a) is already convex downwards. This phenomenon can be confirmed by observing the electromagnetic field distribution at a distance of 90 μm of the measurement object in Figure 6(a), where the light is focused towards the optical axis by the lens. The phase distribution is considered to be a downward convex curve because the phase is larger away from the optical axis, owing to the different optical path lengths between the light from the periphery of the lens, which is further away from the optical axis, and the light near the optical axis. This result is also observed in the phase distribution shown in Figure 6(d). In other words, the phase information based on the shape of the measurement object cannot be properly extracted without processing to cancel the optical path length changes caused by lens focusing. Such processing has been realised in experiments using speckle interferometry.

Figure 9(b) shows the phase distribution when $\alpha = 3\pi/4$ and $\beta = 0$. Since 2π rad corresponds to a wavelength of 532 nm, the phase distribution is converted to a length on the y-axis.

Preprints (www.preprints.org) | NOT PEER-REVIEWED | Posted: 27 October 2023 doi:10.20944/preprints202310.1775.v1

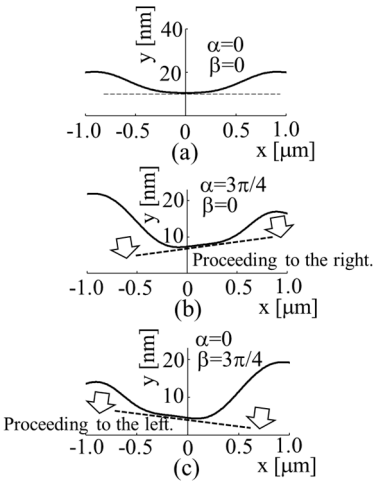

Figure 9. Phase distribution in the case of two light sources at 90μm. (a)Both phase values of α and β are zero rad. (b) α = 3π/4 and β = 0. (c) α= 0 and β = 3π/4.

In this phase distribution as the object light, the angles of α and β are already different, so the phase distribution converted into the length of the measurement result is asymmetrical on the left and right. The distortion of the phase distribution in this oblique direction confirmed that the phases of the two light sources under examination were different. Furthermore, Figure 9(c) shows the result for α=0 and β=3π/4. In this case, the angles of α and β are opposite to the result in Figure 9(b), indicating that an inverse asymmetric phase distribution is obtained.

Figure 10 shows the results of replacing the phase difference with the length when the phase distribution is subtracted Figure 9(a) with both α and β set to 0 from Figure 9(b) and 9(c) with different angles of α and β.

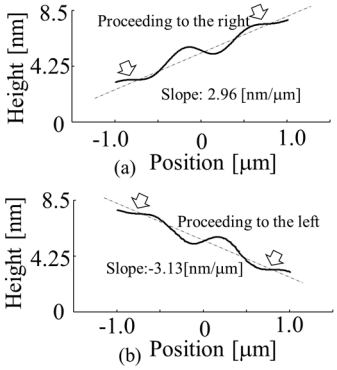

Figure 10. Investigation of the direction of propagation of wavefronts in the case of two light sources with different phases. (a) α = 3π/4 and β = 0 in the case shown in Figure 9(b). (b) α= 0 and β = 3π/4 in the case shown in Figure 9(c).

The different phases of α and β on the left and right in Figs. 10(a) and 10(b), 0 and 3π/4, show that the slope of the detected phase distribution changes from 2.96 [nm/μm], shown in Figure 10(a), where the wavefront travels in the right direction, to -3.13 [nm/μm], shown in Figure 10(b), where the wavefront travels in the left direction. The absolute value of the slope changed slightly, but the sign also changed. The difference between the phases of α and β can be confirmed by checking the phase distribution at 90 μm.

Figure 11 shows the change in the slope of the phase distribution as shown in Figure 10 when the values of phase α and β of the two light sources in Figure 8 are varied as π/4, π/2, and 3π/4, which are set according to the size of the circles and the type of black and white colour, respectively. Then, the case of 0.05, 0.1, 0.2, and 0.5 μm on the horizontal axis of the distance between light sources is investigated. The phase of the two light sources changed, generating a change in the slope of the

Preprints (www.preprints.org) | NOT PEER-REVIEWED | Posted: 27 October 2023 doi:10.20944/preprints202310.1775.v1

wavefront in accordance with the phase difference between the two light sources. Furthermore, the tilt of the wavefront increased with increasing distance between the sources, as shown on the horizontal axis.

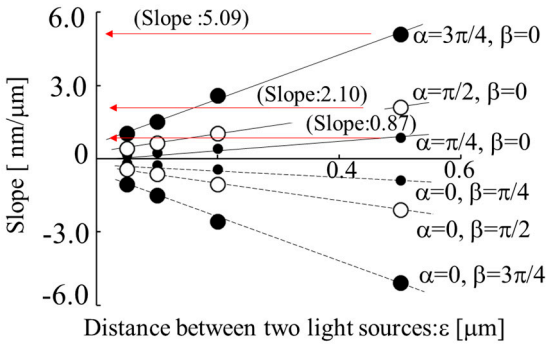

Figure 11. Relation between slope of wavefront of light and distance of light sources with phase at each light source.

In other words, the results in Figure 11 show that the slope of the wavefront varies with changes in the phase of the light source and with the distance between the light sources, which is related to the position of the light source. In this case, according to the calculations presented in this study, because the changes were limited to a minute range, it was found that there is a proportional relationship between the intensity of the light sources and the slope of the wavefront. Furthermore, the changes in the phase of the light sources and the slope of the wavefront shown by the large●, large○ and small● are, for example, (Slope:5.09 nm/μm) for the large●, (Slope:2.10 nm/μm) for the large○ and further (Slope:0.87 nm/μm) for the small● shown in brackets for ε=0.5μm with β=0. It can be seen that the slope is approximately related to the magnitude of the phase α of the light source ($\pi/4$, $\pi/2$, $3\pi/4$).

As shown in Figure 8(a), it can be assumed that the phase distribution of light from the two light sources immediately after passing through the lens contains information regarding the shape of each reflection point on the object. Based on this property, the shape of the microstructure is considered to be detected in the experiment. In other words, it can be confirmed that there is a phase distribution in the zero-order diffracted light as reflected light from microstructures.

3.5. Simulation of different phases from three light sources.

In the previous section, it was confirmed that the zero-order diffracted light from two light sources with different phases in close proximity beyond the diffraction limit contained information about the phases of the two light sources.

Therefore, different phases between the three light sources in close proximity beyond the diffraction limit were further investigated.

In other words, the case where the phase of the light source L1 in the middle is varied on the optical axis as shown in Figure 8(b), with the phase of L2 and L3, which are respectively separated by ε, as 0 rad is considered. In the case of the two light sources in the previous section, when there was a difference in phase between the light sources, it was confirmed that the phase distribution was included in the zeroth-order diffracted light after passing through the lens because of the change in the direction of the wavefront travel. It was investigated whether the phase difference could be detected among the three light sources.

Preprints (www.preprints.org) | NOT PEER-REVIEWED | Posted: 27 October 2023 doi:10.20944/preprints202310.1775.v1

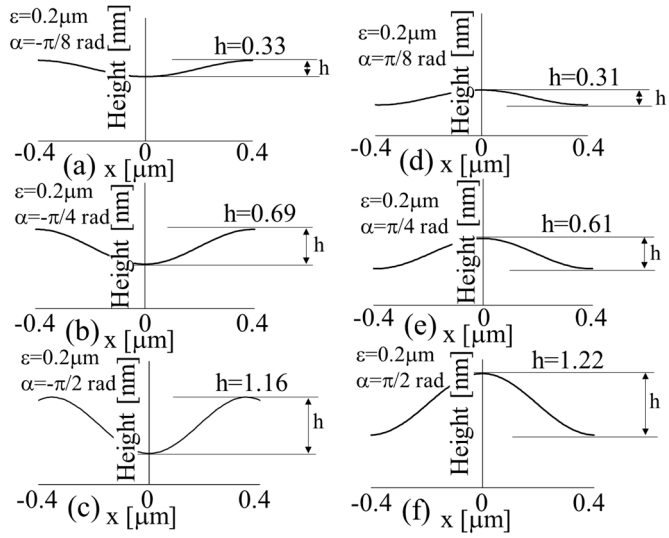

Figure 12. Phase distribution at 90μm in the case of three light sources which midpoint light source (L1) has only phase.

Figures 12(a), 12(b), and 12(c) show the phase distribution at 90 μm when the respective distance between the three light sources is set as ε = 0.2 μm when the phase of L2 and L3 is set as 0 rad and the phase of L1 is set as a negative delayed phase of -π/8, -π/4, and -π/2 rad. The phase of L1 is delayed in comparison with L2 and L3, which confirms that the phase distribution near the optical axis is delayed at 90 μm, resulting in a downward convex result.

In Figure 12, 2π rad corresponds to a wavelength of 532 nm, and the phase difference between the line connecting L2 - L3 and L1 is defined as h_{diff}, which is converted to a length h. In this calculation, the results were considered using the phase distribution obtained by setting the phases of all light sources, L1, L2, and L3, to zero as a standard phase distribution.

First, phases L1, L2, and L3 were set to zero, as shown in Figure 10, and then subtracted from the phase distribution when L1 was changed. On the other hand, Figure 12(d), (e), and (f) are the results of the phase distribution at 90 μm, replaced by the length h, when L1 is set to be phase advanced by setting the phase α to have positive values of π/8, π/4, and π/2 rad compared to L2 and L3.

In this case, in contrast to Figure 12(a), (b), and (c), the phase distribution in the vicinity of the optical axis advances with respect to the surroundings.

The length h is positive, yielding an upward convex result. In this case, the process was also performed by subtracting the reference phase distribution obtained by defining the phase of all light sources as zero. It can be confirmed that the zero-order diffracted light contains phase information of the measurement object with regard to the phases of the three light sources.

The detection of phase components in the zero-order diffracted light is considered to realise super-resolution technology using speckle interferometry.

Figure 13 shows the results of the phase advance and delay states in the near optical axis in the phase difference between L1 and L2, L3 shown on the horizontal axis, converted to the length h, with the parameters of the distance between the light sources ε set to 0.1, 0.2, and 0.5 μm as shown in Figure 12. As the values obtained in the simulations were very small, the characteristics were compared by expressing the length values as a function of the phase change using logarithms. It can be found that the phase change increases as the distance ε between the light sources increases from 0.1 to 0.2 and 0.5 μm. It can also be shown that the detected length h increases as the phase difference increases from π/8, π/4 and π/2 rad. Furthermore, the case where L1, indicated by the white circle, is in a positive phase with respect to L2 and L3 (the shape of the measured object is protruding) is slightly larger than the case where the phase is lagging, indicated by the black circle (the shape of the

Preprints (www.preprints.org) | NOT PEER-REVIEWED | Posted: 27 October 2023 doi:10.20944/preprints202310.1775.v1

measured object is depressed). This indicates that the protruding shape of the measured object is easier to detect. However, the results shown in Figures 12 and 13 are the results of calculations based on simulations, which resulted in the detection of lengths below nm. In particular, in the case of ε = 0.1 μm, where the light sources are close together, the change in length h as the difference between L1 and L2 - L3 is extremely small. As a result of the calculation, the zero-order diffracted light was considered to contain phase information; however, the calculated value was very small.

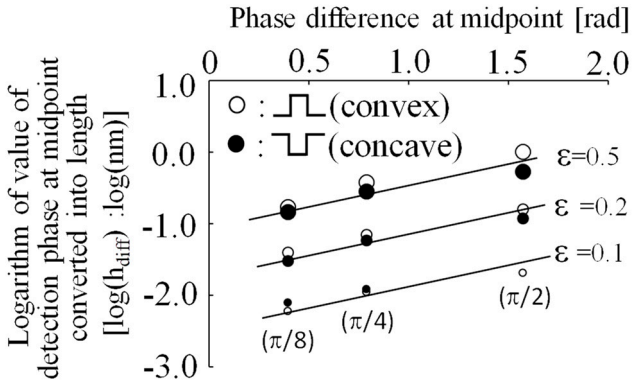

Figure 13. Relation between change of phase of detected midpoint and distance of light sources with phase values. (The phase is converted to length using the relationship between 2π rad and the wavelength (532nm).).

It is thought that this problem should be considered by setting up a pinhole in front of the lens in the simulation to detect only zero-order diffracted light with no spread near the optical axis and by simulating scattered light with a larger number of ray vectors.

In this study, to understand the influence of parameters such as light source spacing on the results, it was decided to examine the results with three light sources using a logarithmic function, which provides a relatively good examination of the phenomenon, rather than directly comparing small arithmetic and large results.

Because it is currently difficult to set up pinholes in optical systems using COMSOL, in the future, consideration is being given to making the use of COMSOL, which is currently being used, more similar to actual optical systems by discussing with software development engineers the creation of pinholes that can prevent complex reflections and interference from occurring in the optical system.

3.6. Observation of an object with periodic structure

By investigating two- and three-light sources, it has been shown that phase information is contained in zero-order diffracted light. Therefore, a measured object with periodicity, as shown in Figure 7, was next considered.

That is, a simulation was performed when an object consisting of 21 light sources with a period of 0.4μm. A phase of each source changes in the range of -π/2 to π/2, which are continuously and closely adjacent at 0.05μm beyond the diffraction limit, as shown by the red dashed line in Figure 14. A phase distribution at a position of 90μm is detected.

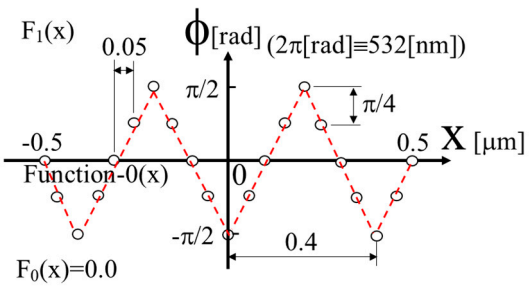

Preprints (www.preprints.org) | NOT PEER-REVIEWED | Posted: 27 October 2023 doi:10.20944/preprints202310.1775.v1

Figure 14. Measurement model with periodical structure based on phase distribution.

In this case, the linearity of the measurement results based on the results shown in Figures 9 and 12 was also considered, and a shape composed of a relatively small phase change was observed.

The results are shown in Figure 15. In this case, the position of 0 on the x-axis corresponds to the position of the optical axis. The phase distribution at 90 μm, which is the standard information, is shown in Figure 15(a) when the phase of all light sources is set to 0 rad, in the same way as in the 2- and 3-light source cases. In this case, the phase distribution is also converted to a length h by replacing 2π rad with a wavelength of 532 nm, and the value is shown in round brackets.

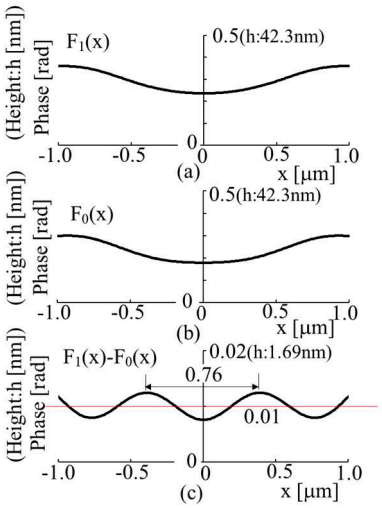

Figure 15. Measured results of the measurement model. (a) Standard phase distribution by setting phase value of all points making as 0 rad. (b) Measured results including standard phase distribution. (c) Measurement results with standard phase distribution eliminated.

Figure 15(b) shows the phase distribution detected at 90 μm as well, with the phase set at each of the 21 points shown in Figure 14. The result obtained by subtracting the standard phase distribution in Figure 15(a) from that in Figure 15(b) is shown in Figure 15(c). In this case, the phase distribution according to the sinusoidal shape shown in Figure 14 is shown in Figure 15(c), although the phase change is very small. In this case, the detected sinusoidal bias component (indicated by the red line) is not necessarily 0, as shown in Figure 14, but is 0.01 rad because the phase distribution is at 90 μm as the detection position. It is not possible to investigate precisely whether this result is presently caused by the value of the optical path length to 90 μm from the measurement object surface since the light passed through the lens.

Even for phase distributions that are more complicated than the two- and three-light sources, as shown in Figure 15(c), the phase information is maintained within the zeroth-order diffracted light, and the shape of the original phase distribution can be retrieved after passing through the lens. In this case, the length at which a change is extracted is small. In addition, the period of the phase distribution shown in Figure 15(c) is slightly larger, 0.76 μm, while the period of the periodic structure shown in Figure 14 is 0.4 μm. Although the magnification was originally supposed to be 1.2x based on the positional relationship between the position of the measurement object and the imaging plane, the magnification was larger than that. The zero-order diffracted light shows a slight spread immediately after emitting from the light source, and although the beam is converging after passing through the lens, it still reaches 90 μm in a spreading state. Because the beam was slightly wider than the object to be measured, it was assumed that the phase distribution (shape distribution) was wider than 0.4μm. This phenomenon can be observed in the region around 90 μm in Figure 6(a).

This problem is considered to be similar to the situation in the experimental results shown in Figure 7, where a diffraction grating with a period of 278 nm was measured, and the measurement result was detected with a magnification of approximately 300 nm. This phenomenon of

magnification change has often been observed in previous experiments. If this phenomenon can be corrected by setting up a pinhole in the simulation and if information can be extracted only in the area near the optical axis, it is possible that the change in magnification can be improved by collecting information at a position closer to the image formation position. In the future, it will be necessary to develop a super-resolution technology using the phase distribution based on more careful consideration by reexamining the simulation model using pinholes and scattered light.

However, to observe microstructures, situations exist where an objective must be used to magnify the image. In this case, only information near the lens optical axis needs to be extracted by pinhole, and as shown in Figure 6, the situation where the magnification changes could be improved if the information is collected closer to the image formation position from the current 90 μm detection position. In the future, it will be necessary to investigate the situation in which measurement sensitivity and magnification change with respect to the detection position of the information in detail.

In this study, by detecting the phase distribution of light using a simulation, it was clarified that the optical explanation for the realisation of super-resolution is the conservation of the phase distribution with respect to the shape of the measurement object in the zero-order diffracted light.

4. Conclusion

The conventional concept of diffraction limit associated with diffraction by Abbe and Rayleigh is based solely on the intensity distribution of light. In this situation, among the diffracted light generated when the microstructures are illuminated, higher-order diffracted light, except for zero-order diffracted light, cannot pass through the lens aperture, according to Abbe's image formation theory. Therefore, it was believed that they could not be resolved in the imaging plane.

However, the phase distribution analysis performed in this study shows that the zeroth-order diffracted light passes through the lens and that there is phase information in the zeroth-order diffracted light, as shown in this study. As a result, it was confirmed in this study that the observation of microstructures beyond the diffraction limit is realised by detecting the phase information contained in zeroth-order diffracted light with high resolution based on speckle interferometry.

In the future, a new simulation model that more closely imitates an actual optical system will be created, and a simulation using scattered light and extracting only zeroth-order diffracted light owing to pinholes will be performed.

Funding: This research was funded by JSPS KAKENHI, Grant Number 20H02165.

Institutional Review Board Statement: Not applicable

Informed Consent Statement: Not applicable.

Acknowledgments: We would like to thank Dr. Dahai Mi of Keisoku Engineering System CO.LTD for his kind guidance and support in the use of COMSOL Multiphysic.

Conflicts of Interest: The authors declare no conflict of interest.

References

1. Betzig E.; et al. Imaging intracellular fluorescent proteins at nanometer resolution. *Science* **2006**, 313, 1642–1645.
2. Hell S. W.; Wichmann J. Breaking the diffraction resolution limit by stimulated emission: stimulated-emission-depletion fluorescence microscopy. *Optics Letters* **1994**, 19, 780-782.
3. Klar T. A.; Jakobs S.; Dyba M.; Egner A.; Hell S.W. Fluorescence microscopy with diffraction resolution barrier broken by stimulated emission. *Proc. Natl. Acad. Sci.* **2000**, 97, 8206–8210. [https://doi.org/10.1073/pnas.97.15.8206]
4. Garini Y.; Vermolen B. J.; Young I. T. From micro to nano: recent advances in high-resolution microscopy. *Current Opinion in Biotechnology* **2005**, 16, 3-12.
5. Neice A. Chapter 3 - Methods and Limitations of Subwavelength Imaging. *Adv. in Image. and El. Phys.* **2010**, 163, 117–140. [https://doi.org/10.1016/S1076-5670(10)63003-0]
6. Haeberle O.; Belkebir K.; Giovaninni H.; Sentenac, A. Tomographic Diffractive Micros-copy: Basics, Techniques and Perspectives. *J. Mod. Opt.* **2010**, 57, 686–699. [doi:10.1080/09500340.2010.493622]

7. Hess T. S.; Girirajan P. K. T.; Mason D. M. Ultra-high resolution imaging by fluorescence photoactivation localization mi-croscopy. *Biophys.* **2006**, 91, 4258-4272.
8. Huang B. Super-resolution optical microscopy: multiple choices. *Current Opinion in Chemical Biology* **2010**,14, 10-14.
9. Rust M. J.; Bates M.; Zhuang X. Sub-diffraction-limit imaging by stochastic optical re-construction microscopy (STORM), *Nature Methods* **2006**, 3, 793–795.
10 Heilemann M.; et al. Subdiffraction-resolution fluorescence imaging with conventional fluorescent probes. *Angew Chem. Int. Ed Engl*. **2008**, 47, 6172–6176.
11 Heintzman R.; Ficz G. Beaking the resolution limit in light microscopy. *Briefing in functional genomics and proteomics*. **2006**, 5, 289-301.
12 Gudiksen M. S.; et al. Growth of nanowire superlattice structures for nanoscale photonics and electronics, *Nature*, **2002**, 415, 617-620.
13. Garnett E.; Mai L.; Yang P. Introduction: 1D Nanomaterials/Nanowires, *Chem. Rev*., **2019**, 119, 8955-8957, [doi.10.1021/acs.chemrev.9b00423]
14. Kohler H. On Abbe's theory of image formation in the microscope. *Optica Acta*, **1981**, 28,1691-1701.
15. Born M.; Wolf E. *Principles of optics 7th ed.*; Cambridge University Press; Cambridge, UK; 2019, pp.167-177, pp.290-292, and pp.370-374.
16. Hecht E.; *Optics 4th ed.*; Addison-Wesley Publishing Co.; San Francisco, USA; 2002, pp.24-31, pp.149-165, pp.393-400, and pp.467-474.
17. Arai Y. Three-dimensional shape measurement beyond the diffraction limit of lens. *J. Mod. opt*., **2018**, 65, 1866-1874. [doi.org/10.1080/09500340.2018.1470266].
18. Cloud G. *Optical Methods of Engineering Analysis*. Cambridge University Press; New York, USA, 1995; pp.395-476.
19. Malacara D. *Optical Shop Testing*. John Wiley &Sons; New York, 1992; pp.501-652.
20. Sirohi R. S. *Speckle Metrology*. Marcel Dekker; New York, USA, 1993; pp.99-234.
21. Arai Y. Consideration of existence of phase information of object shape in zeroth-order diffraction beam using electromagnetic simulation with aperture in front of object. *J. Mod. Opt.* **2020**, 67, 523-530. [doi.org/10.1080/09500340.2020.1760383].
22. Arai Y. Electronic Speckle Pattern Interferometry based on spatial information using only two sheets of speckle patterns, *J. Mod Opt*., **2014,** 61, 297-306.
23. Arai Y. Microshape measurement method using speckle interferometry based on phase analysis, *Photonics*, **2021**, 8, [doi.org/10.3390/photonics8040112].
24. Arai Y. Observation of micro-characters using three-dimensional shape measurement method based on speckle interferometry, *J. Mod. Opt*., **2020**, 67,1451-1461. [doi.org/10.1080/09500340.2020.1864041]
25. Arai Y.; Chen T. Simulation-based considerations on the Rayleigh Criterion in super-resolution techniques based on speckle interferometry, *Photonics*, **2023**, 10, 374. [https://doi.org/10.3390/photonics10040374]
26. Maslov A.V.; Astratov V.N. Imaging of sub-wavelength structures radiating coherently near microspheres, *Appl. Phys. Lett*., **2016**, 108, 051104, [https://doi.org/10.1063/1.4941030]
27. Kassamakov I.; Lecler S.; Nolvi A.; Leong-Hoi A.; Montgomery P.; Haeggstrom E. 3D Super-Resolution Optical Profiling Using Microsphere Enhanced Mirau Interferometry, *Sci. Reports* **2017**, 7, 3683. [doi:10.1038/s41598-017-03830-6]
28. Pendy J. B. Negative refraction makes a perfect lens. *Phy. Rev. Lett.* **2000**, 85, 3966-3969.